LETTER

doi:10.1038/nature09618

Ice–sheet acceleration driven by melt supply variability

Christian Schoof[1]

Increased ice velocities in Greenland[1] are contributing significantly to eustatic sea level rise. Faster ice flow has been associated with ice–ocean interactions in water-terminating outlet glaciers[2] and with increased surface meltwater supply to the ice-sheet bed inland. Observed correlations between surface melt and ice acceleration[2–6] have raised the possibility of a positive feedback in which surface melting and accelerated dynamic thinning reinforce one another[7], suggesting that overall warming could lead to accelerated mass loss. Here I show that it is not simply mean surface melt[4] but an increase in water input variability[8] that drives faster ice flow. Glacier sliding responds to melt indirectly through changes in basal water pressure[9–11], with observations showing that water under glaciers drains through channels at low pressure or through interconnected cavities at high pressure[12–15]. Using a model that captures the dynamic switching[12] between channel and cavity drainage modes, I show that channelization and glacier deceleration rather than acceleration occur above a critical rate of water flow. Higher rates of steady water supply can therefore suppress rather than enhance dynamic thinning[16], indicating that the melt/dynamic thinning feedback is not universally operational. Short-term increases in water input are, however, accommodated by the drainage system through temporary spikes in water pressure. It is these spikes that lead to ice acceleration, which is therefore driven by strong diurnal melt cycles[4,14] and an increase in rain and surface lake drainage events[8,17,18] rather than an increase in mean melt supply[3,4].

The effective pressure in the subglacial drainage system, defined as overburden minus basal water pressure, controls coupling between ice and bed: lower effective pressure weakens the ice–bed contact and permits faster sliding[9–11]. Effective pressure is controlled by subglacial drainage, which occurs through two principal types of conduit (Fig. 1): Röthlisberger channels[19,20] are kept open by a balance between a widening of the channel by wall melting due to heat dissipation in the water flow, and a narrowing that results from the inward creeping motion of the surrounding ice. By contrast, cavities[11,21,22] are formed where ice is forced upwards by horizontal sliding over protrusions on the glacier bed. This opens a gap in the lee of the protrusion, with gap size controlled by the opening rate due to sliding and by creep closure of the cavity roof.

An increase in effective pressure leads to faster creep closure. In an equilibrium channel, this must be balanced by greater wall melt. Greater wall melt in turn requires higher discharge and, thus, a larger channel. Röthlisberger channels therefore increase in size with increasing effective pressure (decreasing water pressure). This causes water flow from smaller channels into larger ones, favouring the formation of an arterial network with few main channels at low water pressure[19,23]. Cavities differ from channels as their size is not controlled by wall melt and increases rather than decreases with water pressure. A reduction in effective pressure suppresses creep closure and allows larger cavities to form[11,22]. This favours macroporous behaviour[24] with spatially distributed drainage along the ice–bed interface and water discharge increasing with water pressure. The abundance of channels relative to cavities therefore determines whether water pressure is low or high in the steady state: channels can efficiently transport water at high effective pressure whereas cavities require low effective pressure to transport the same flux. Past models[23,25], however, do not capture switches from cavities to channels in spatially extended drainage or the formation of an arterial network, and cannot predict the spatial configuration of the drainage system.

Here I unify the description of cavities and channels and predict how spatially extended drainage systems can switch from cavities to channels and back. The basic physics of cavities and channels can be captured in a single equation for the cross-sectional area, S, of a subglacial conduit, which can be a channel or cavity (Supplementary Information and Fig. 1):

$$\frac{\mathrm{d}S}{\mathrm{d}t} = c_1 Q\Psi + u_b h - c_2 N^n S \qquad (1)$$

where Q is the water discharge, Ψ is the hydraulic gradient along the conduit and $N = p_i - p_w$ is the effective pressure in the conduit (ice

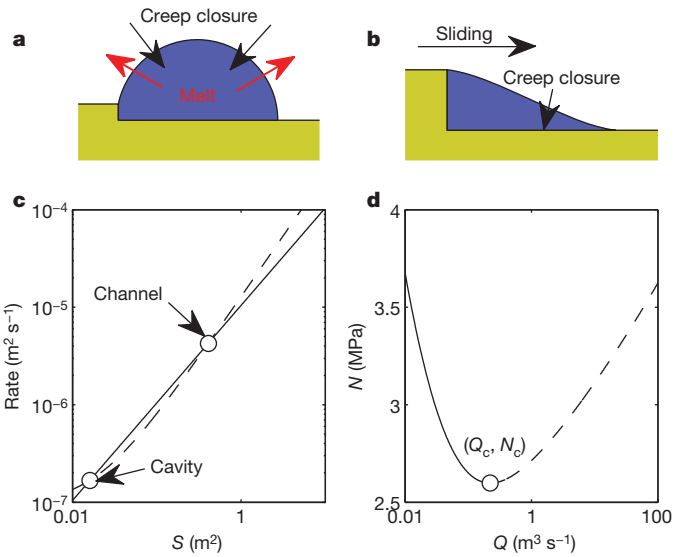

Figure 1 | Properties of a single conduit. **a**, **b**, Physics of channels (**a**) and cavities (**b**). **c**, Conduit opening rate, $c_1 Q\Psi + u_b h$ (dashed line), and closure rate, $c_2 N^n S$ (solid line), plotted against S. **d**, Steady-state N versus Q in a conduit (equation (2)). Parameter values are given in Methods Summary. Each conduit can generally attain one of two equilibria (points of intersection given as circles in **c**). These can be identified as channel and cavity. The larger (channel) equilibrium is prone to instability[20]: if perturbed to slightly larger size, the conduit will continue to grow (opening rate exceeds closing rate to the right of the intersection). In a network of conduits, this eventually leads to one channel growing at the expense of all other nearby ones. The cavity equilibrium, by contrast, is stable, and cavities of similar size can coexist. In the steady state, effective pressure increases with discharge in a channel (increasing N makes the closure curve steeper, moving the channel intersection in **c** to larger values of S), and decreases with discharge in a cavity. A conduit becomes a channel above a critical discharge, Q_c (dashed curve in **d**), and remains a cavity below Q_c.

[1]Department of Earth and Ocean Sciences, University of British Columbia, 6339 Stores Road, Vancouver, British Columbia V6T 1Z4, Canada.

overburden, p_i, minus water pressure, p_w). Q is related to S and Ψ through the Darcy–Weisbach law[26], $Q = c_3 S^{\alpha} |\Psi|^{-1/2} \Psi$, where $\alpha = 5/4$ and c_3 is related to the Darcy–Weisbach friction factor. The first term in equation (1) is the rate of conduit opening due to wall melting, the second is the rate of opening due to sliding of ice at speed u_b over bed protrusions of size h and the third is conduit roof closure due to viscous creep; c_1, c_2 and n are constants related to the latent heat of fusion and ice viscosity.

In the steady state, the effective pressure and discharge in a conduit are then related through (Fig. 1d)

$$N^n = \frac{c_1 Q \Psi + u_b h}{c_2 c_3^{-1/\alpha} Q^{1/\alpha} \Psi^{-1/(2\alpha)}} \quad (2)$$

At low discharge, Q, the effective pressure, N, decreases with Q, as is expected for cavities, whereas at higher discharge, N increases with Q and the conduit behaves as a Röthlisberger channel. The switch-over in behaviour occurs at a critical discharge

$$Q_c = \frac{u_b h}{c_1 (\alpha - 1) \Psi}$$

Below Q_c, the conduit is kept open mainly by ice flow over bed protrusions; above Q_c, it is kept open by wall melting.

A linear stability analysis (Supplementary Information) also shows that discharge becomes concentrated into a few conduits when the mean water discharge through an array of laterally connected conduits exceeds Q_c: driven by wall melting, a single conduit will grow into a large channel (with the properties of a Röthlisberger channel, its size, S,

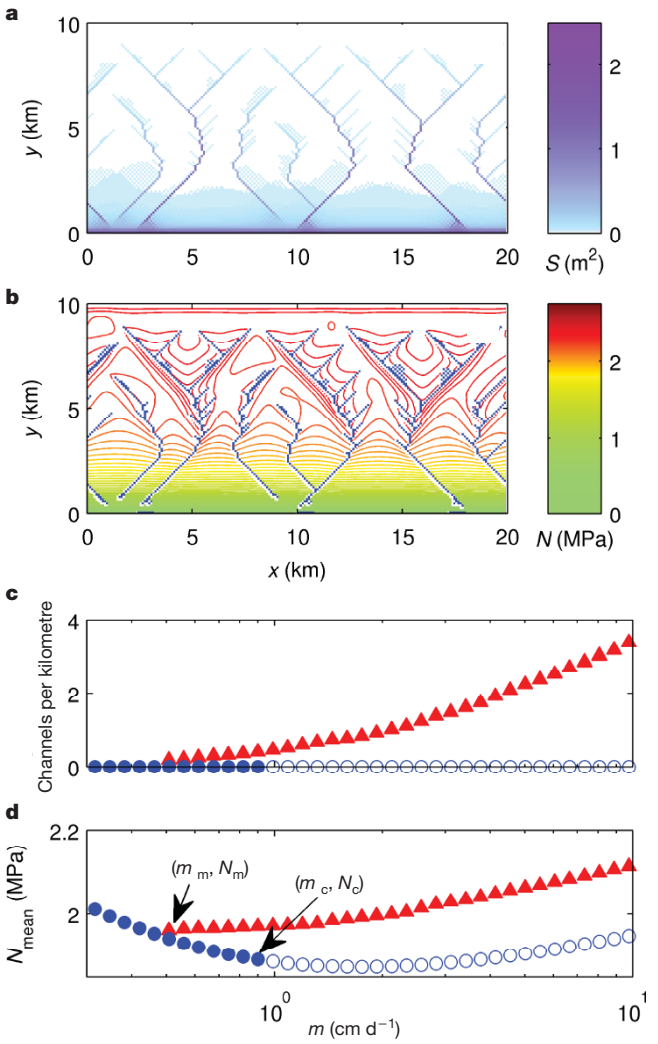

Figure 2 | Steady-state drainage systems. **a**, **b**, Example of a drainage system formed spontaneously through the channelizing instability. **a**, Conduit sizes. Channels are much larger (dark blue and purple) than the surrounding cavities. **b**, Channels are shown in blue and effective pressure contours are shown at 0.05-MPa intervals. The pressure distribution reveals how channel–cavity interactions control the drainage pattern. Channels are at higher effective pressure than the surrounding cavities. Local water pressure maxima (minima of N) separate the channels, driving water flow towards them. **c**, **d**, Steady-state drainage system characteristics as functions of water supply rate, m. **c**, Channel density (average number of channels per unit width of the domain) plotted against m. **d**, Mean of N over the domain plotted against m. Red triangles correspond to channelized systems; blue circles correspond to unchannelized ones. Open circles show unstable unchannelized systems (which will evolve into a channelized state if perturbed). Instability first occurs at a critical water supply, m_c, corresponding to a critical discharge, Q_c. Mean effective pressure decreases with water supply (and, hence, discharge) for stable unchannelized systems, and increases with water supply for channelized ones. For some intermediate values of m (between m_c and a lower limit, m_m, that corresponds to a critical lower discharge, Q_m), both channelized and unchannelized states are possible: their low water pressure allows channels to suck in enough water to keep themselves open, but the discharge through the system is too low for an unchannelized system to channelize spontaneously. A video animation is included in Supplementary Information.

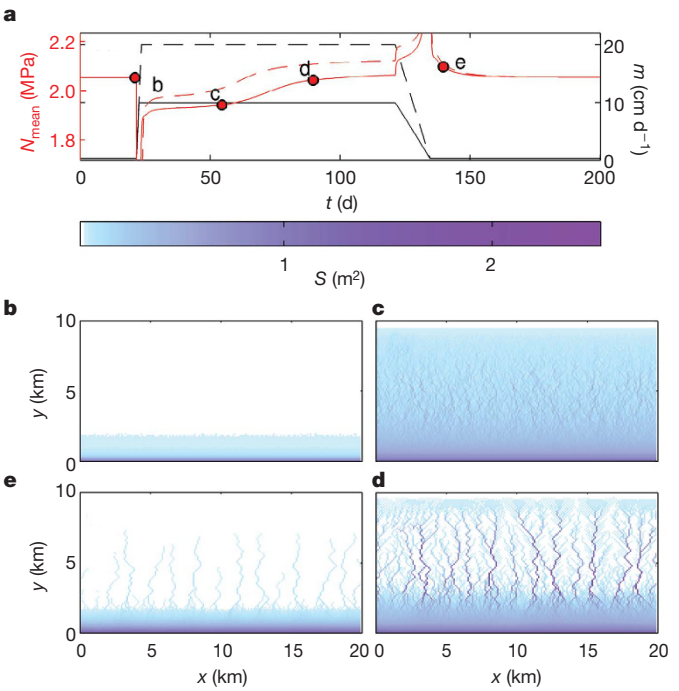

Figure 3 | Idealized seasonal evolution of the drainage system. **a**, The spatial mean of effective pressure, N (red lines), plotted against time. The simulations shown are forced by a sharp increase (over 1 d) in water supply, m (black line), from a wintertime value of 0.33 cm d^{-1} to a summertime value of 10 cm d^{-1} (solid lines) and 20 cm d^{-1} (dashed lines). This is followed by steady supply for 100 d and a gradual return to 0.33 cm d^{-1}. The dots marked b–e correspond to the spatial drainage configurations shown in panels **b**–**e**, respectively. **b**–**e**, The drainage system starts close to an unchannelized steady state with small conduits (**b**). The abrupt increase in m leads to a sharp drop in effective pressure (a 'spring event'[9]), which opens the drainage conduits to accommodate the additional discharge but does not immediately channelize the system (**c**). Efficient channelization causes effective pressure to increase only after some time (**d**), reaching values above those of wintertime. The final drop in m causes a temporary jump in effective pressure that leads the system to shut down for winter (**e**). Both simulations in panel **a** show qualitatively the same response. However, the larger jump in water supply (dashed lines in **a**) leads to a shorter and less pronounced period of low effective pressure than the smaller jump (solid lines in **a**). A video animation is included in Supplementary Information.

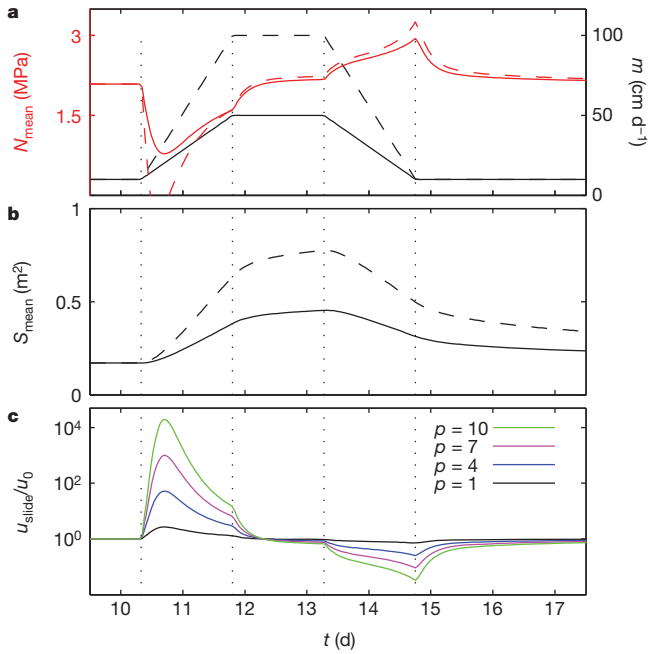

Figure 4 | Temporal variations in water input. **a**, The mean of N (red) over the domain plotted against time for two different simulations. Simulations are started from a steady-state channelized system and forced with time-dependent but spatially uniform water input, m (black), imposing fivefold (solid lines) and tenfold (dashed lines) increases in m over 4 d. **b**, The spatial mean of conduit size, S, plotted against time. During the initial increase in water input, conduits have not yet been able to widen to accommodate increased discharge. To force the additional discharge instead requires a temporary spike in hydraulic gradient, Ψ, leading to higher water pressure (lower N) upstream of the margin (red lines). This temporary drop in N is stronger for bigger jumps in m (dashed lines in **a**): N_{mean} can even drop to zero, which corresponds to complete decoupling between ice and bed. Hydrofracture should occur[30], although this is not included in my model. After the initial transient, conduit size adjusts and effective pressure increases again, reaching a maximum when m decreases again. **c**, Modelled sliding velocity, u_{slide}, normalized by steady-state sliding velocity, u_0. Time series of u_{slide}/u_0 are shown corresponding to the solid curves in **a** and **b**. Sliding is modelled using the empirical relation[9,23] $\tau_b = Cu_{slide}^{1/p}N$, where τ_b is driving stress in the ice and C and p are constant parameters (Supplementary Information). The curves correspond to different values of the sliding-law nonlinearity, p, as indicated. In all cases, the initial drop in N leads to fast sliding. Recent developments[10,11] in glacier sliding suggest large values for p, for which the magnitude of sliding events is more pronounced. The calculation for u_{slide}, however, excludes the effects of stress transfer to other parts of the glacier, which would prevent excessively large sliding velocities.

and effective pressure, N, increasing with discharge, Q) at the expense of nearby ones, which shrink to form smaller cavities. Below this critical mean discharge, all conduits can be stable at the same size and behave as cavities (in which the steady-state effective pressure decreases with increasing discharge).

The nonlinear dynamics of channelization can be captured by considering a network[26] of conduits described by equation (1) (Methods and Supplementary Information). With mean discharge below a critical value, Q_c, an initially nearly uniform network remains uniform as predicted by linear stability analysis. For a mean discharge level greater than Q_c, the channelizing instability occurs and the system spontaneously evolves a set of large, well-defined channels fed by smaller ones that are separated in turn by cavities (Fig. 2). This effect is similar to melt channelization in magmatic systems[27]. The spacing between the channels is controlled by lateral effective pressure gradients and decreases with increasing water input. An important feature of the nonlinear system is that channelization is irreversible. Even if the mean discharge is dropped back below Q_c, the previously formed channels do not necessarily disappear: this requires discharge to drop below a lower critical level, Q_m (Fig. 2).

An increase in steady meltwater supply lowers the effective pressure and therefore speeds up sliding[9–11] only below the critical discharge, Q_c, for channelization (equation (2); Figs 1d and 2d). Once this is exceeded, the effective pressure increases again. Channelization increases the effective pressure further: concentrated discharge leads to faster channel wall melting that must be offset by stronger creep closure, driven by increased N. An increase in steady meltwater input therefore has limited potential to cause glacier acceleration and will eventually even lead to glacier deceleration.

This result, however, applies only to steady conditions. Observations in Greenland[6] indicate that seasonal and short-term water supply variations can lead to transient acceleration. Ice velocities in some areas are consistently above their wintertime average early in the melt season, but slow down to below their wintertime average later in summer. This can be explained by a seasonal switch from unchannelized to channelized drainage, in which a combination of increased water supply and incomplete channelization cause low effective pressures in early summer (Fig. 3). However, Fig. 3 also shows that channelization occurs faster and that the decrease in effective pressures early in the melt season is smaller when summertime water supply rates are large. Higher summer surface melt rates are therefore likely to suppress the magnitude and duration of the period of higher velocities in early summer.

Short-term spikes in water supply can also induce spikes in water pressure, and lead to the observed[6] short-term ($\lesssim$1-day) fast-sliding episodes even when the drainage system has channelized[13] (Fig. 4). This happens because the size of conduits adjusts slowly (over several days), and the drainage system does not have the capacity to accommodate sudden extra water throughput except by an increase in the hydraulic gradient, Ψ. This increase in Ψ requires higher water pressures in the interior of the drainage system, leading to lower effective pressures and, hence, to faster sliding. Not only can short-term variability lead to acceleration even after channelization, but the magnitude of water pressure excursions during short-term water supply spikes can also be much larger than the slower seasonal water pressure signal (compare Figs 3a and 4a).

Ice velocity can therefore respond much more to short-term temporal variations in water supply than to changes in mean water flow. This has major implications for ice-sheet dynamics and feedbacks between surface melting and dynamic thinning[7]. More surface water input through melt or rain is likely if dynamic thinning draws down the ice surface. This can lead to increased ice flow and further thinning if the basal water supply is initially very low or if the bed is frozen. However, larger rates of summer water supply can also cause faster channelization and potential ice deceleration. Further acceleration must then be driven instead by short-term temporal variability in water supply. This is favoured by strong diurnal cycles[5] and frequent rain events[17], both of which are more likely at lower latitudes, or if the ice sheet develops numerous surface lakes that drain abruptly[18].

Drainage channelization under glaciers and ice sheets suppresses the ability of steady surface water supply to cause further ice acceleration, but faster ice flow can be caused instead by water input variations[8]. This is already observable in Greenland and will become more important when the climate changes: diurnal melt cycles already contribute to ice flow in southern Greenland[5], and more frequent rain events are predicted to result from a northward shift of storm tracks over the next century[28], which will cause further ice acceleration. My results are also relevant to palaeo-ice-sheet dynamics. Simulations that do not include subglacial processes cannot explain the observed rapid collapse of the Laurentide ice sheet[29]. A water input/dynamic thinning feedback is a plausible collapse mechanism, driven by rain and diurnal melt cycles rather than by mean melt alone. Future coupled models are needed to fully explain the role of drainage in rapid deglaciation, and my results show that channelization and short-term drainage variability are the crucial processes that must be captured in these models.

METHODS SUMMARY

I model a drainage network in which nodes i and j are connected by a conduit (network edge) labelled by subscripts i and j. The conduit evolves according to

$$\frac{dS_{ij}}{dt} = c_1 Q_{ij} \Psi_{ij} + u_b h - c_2 N_{ij}^n S_{ij}$$

where S_{ij}, Q_{ij}, Ψ_{ij} and N_{ij} are conduit size, flux, hydraulic gradient and effective pressure, respectively. Conduit sizes, S_{ij}, and effective pressures at the nodes, N_i, are the primary variables. I set $\Psi_{ij} = \Psi_{ij}^0 + (N_j - N_i)/L_{ij}$, where L_{ij} is the distance between nodes and Ψ_{ij}^0 is a geometrically controlled background hydraulic gradient (Supplementary Information). Additionally, $N_{ij} = (N_i + N_j)/2$ and $Q_{ij} = c_3 S_{ij}^{\alpha} |\Psi_{ij}|^{-1/2} \Psi_{ij}$. At each node, mass is conserved. Ignoring water storage (Supplementary Information), mass conservation requires that

$$\sum_j Q_{ij} = m_i$$

where the sum is over the nodes, j, connected to the node i, and m_i is water input to node i. I use a rectangular lattice network oriented at 45° to downslope, with a domain size of 10 km × 20 km and 2×10^4 conduits. I impose $N = 0$ at the margin, zero inflow upstream and periodic sides. Water input is spatially uniform (all m_i are the same) and is given as rate of volume input per unit area. The parameters are $\alpha = 5/4$, $c_1 = 3.4 \times 10^{-9}\,\mathrm{Pa}^{-1}$, $c_2 = 4.5 \times 10^{-25}\,\mathrm{Pa}^{-3}\,\mathrm{s}^{-1}$, $c_3 = 0.33\,\mathrm{kg}^{-1/2}\,\mathrm{m}^{3/2}$ and $u_b h = 3\,\mathrm{m}^2\,\mathrm{yr}^{-1}$ (Supplementary Information). For illustrative purposes, Ψ_{ij}^0 is based on the shape of a plastic glacier with a yield stress of 10^5 Pa on a 3° slope. In Fig. 1 $\Psi = 512\,\mathrm{Pa\,m}^{-1}$ and $u_b h = 3\,\mathrm{m}^2\,\mathrm{yr}^{-1}$, and in Fig. 1c $N = 2.85$ MPa.

Received 26 April; accepted 25 October 2010.

1. Rignot, E. & Kanagaratnam, P. Changes in the velocity structure of the Greenland ice sheet. *Science* **311,** 986–990 (2006).
2. Joughin, I. *et al.* Seasonal speedup along the western flank of the Greenland ice sheet. *Science* **320,** 781–783 (2008).
3. Zwally, H. J. *et al.* Surface-melt induced acceleration of Greenland ice-sheet flow. *Science* **5579,** 218–222 (2002).
4. van de Wal, R. S. W. *et al.* Large and rapid melt-induced velocity changes in the ablation zone of the Greenland ice sheet. *Science* **321,** 111–113 (2008).
5. Shepherd, A. *et al.* Greenland ice sheet motion coupled with daily melting in late summer. *Geophys. Res. Lett.* **36,** L01501 (2009).
6. Bartholomew, I. *et al.* Seasonal evolution of subglacial drainage and acceleration in a Greenland outlet glacier. *Nature Geosci.* **3,** 408–411 (2010).
7. Parizek, B. R. & Alley, R. B. Implications of increased Greenland surface melt under global-warming scenarios: ice-sheet simulations. *Quat. Sci. Rev.* **23,** 1013–1027 (2004).
8. Bartholomaus, T. C., Anderson, R. S. & Anderson, S. P. Response of glacier basal motion to transient water storage. *Nature Geosci.* **1,** 33–37 (2008).
9. Iken, A. & Bindschadler, R. A. Combined measurements of subglacial water pressure and surface velocity of Findelengletscher, Switzerland: conclusions about drainage system and sliding mechanism. *J. Glaciol.* **32,** 101–119 (1986).
10. Iverson, N. R., Baker, R. W., Hooke, R. LeB., Hanson, B. & Jansson, P. Coupling between a glacier and a soft bed: I. A relation between effective pressure and local shear stress determined from till elasticity. *J. Glaciol.* **45,** 31–40 (1999).
11. Schoof, C. The effect of cavitation on glacier sliding. *Proc. R. Soc. Lond. A* **461,** 609–627 (2005).
12. Kamb, B. *et al.* Glacier surge mechanism: 1982–1983 surge of Variegated Glacier, Alaska. *Science* **227,** 469–479 (1985).
13. Iken, A., Echelmeyer, K. A., Harrison, W. D. & Funk, M. Mechanisms of fast flow in Jakobshavns Isbrae, Greenland, part I: measurements of temperature and water level in deep boreholes. *J. Glaciol.* **39,** 15–25 (1993).
14. Hubbard, B., Sharp, M. J., Willis, I. C., Nielsen, M. K. & Smart, C. C. Borehole water-level variations and the structure of the subglacial hydrological system of Haut Glacier d'Arolla, Valais, Switzerland. *J. Glaciol.* **41,** 572–583 (1995).
15. Lappegard, G., Kohler, J., Jackson, M. & Hagen, J. O. Characteristics of subglacial drainage system deduced from load-cell measurements. *J. Glaciol.* **52,** 137–147 (2006).
16. Magnusson, E., Björnsson, H., Rott, H. & Palsson, F. Reduced glacier sliding caused by persistent drainage from a subglacial lake. *Cryosphere* **4,** 13–20 (2010).
17. Howat, I. M., Tulaczyk, S., Waddington, E. & Björnsson, H. Dynamic controls on glacier basal motion inferred from surface ice motion. *J. Geophys. Res.* **113,** F03015 (2008).
18. Das, S. B. *et al.* Fracture propagation to the base of the Greenland ice sheet during supraglacial lake drainage. *Science* **320,** 778–781 (2008).
19. Röthlisberger, H. Water pressure in intra- and subglacial channels. *J. Glaciol.* **11,** 177–203 (1972).
20. Nye, J. F. Water flow in glaciers: jökulhlaups, tunnels and veins. *J. Glaciol.* **17,** 181–207 (1976).
21. Walder, J. Hydraulics of subglacial cavities. *J. Glaciol.* **32,** 439–445 (1986).
22. Kamb, B. Glacier surge mechanism based on linked cavity configuration of the basal water conduit system. *J. Geophys. Res.* **92,** 9083–9100 (1987).
23. Fowler, A. C. Sliding with cavity formation. *J. Glaciol.* **33,** 255–267 (1987).
24. Lüthi, M., Funk, M., Iken, A., Gogineni, S. & Truffer, M. Mechanisms of fast flow in Jakobshavns Isbrae, Greenland, part III: measurements of ice deformation, temperature and cross-borehole conductivity in boreholes to the bedrock. *J. Glaciol.* **48,** 369–385 (2002).
25. Hewitt, I. J. & Fowler, A. C. Seasonal waves on glaciers. *Hydrol. Process.* **22,** 3919–3930 (2008).
26. Clarke, G. K. C. Lumped-element analysis of subglacial hydraulic circuits. *J. Geophys. Res.* **101,** 17547–17559 (1996).
27. Hewitt, I. J. & Fowler, A. C. Melt channelization in ascending mantle. *J. Geophys. Res.* **114,** B06210 (2009).
28. Schuenemann, K. C. & Cassano, J. J. Changes in synoptic weather patterns and Greenland precipitation in the 20th and 21st centuries: 2. Analysis of 21st century atmospheric changes using self-organizing maps. *J. Geophys. Res.* **115,** D05108 (2010).
29. Tarasov, L. & Peltier, W. R. Terminating the 100 kyr ice age cycle. *J. Geophys. Res.* **102,** 21665–21693 (1997).
30. Tsai, V. C. & Rice, J. R. A model for turbulent hydraulic fracture and application to crack propagation at glacier beds. *J. Geophys. Res.* **115,** F03007 (2010).

Supplementary Information is linked to the online version of the paper at www.nature.com/nature.

Acknowledgements Thanks to G. Clarke, T. Creyts, G. Flowers, I. Hewitt, R. Hindmarsh, M. Jellinek and V. Radić for comments on the manuscript, and to C. Koziol and M. Jaffrey for discussions. Financial support was provided by the Canada Research Chairs Program, NSERC Discovery Grant 357193-08 and the Canadian Foundation for Climate and Atmospheric Science through the Polar Climate Stability Network.

Author Information Reprints and permissions information is available at www.nature.com/reprints. The author declares no competing financial interests. Readers are welcome to comment on the online version of this article at www.nature.com/nature. Correspondence and requests for materials should be addressed to the author (cschoof@eos.ubc.ca).